Isostatic Flexure of a Finite Slope Due to Sea-Level Rise and Fall

E. W. H. Hutton and J. P. M. Syvitski

Community Surface Dynamics Modeling System,
INSTAAR, University of Colorado
Boulder, CO

A. B. Watts

Department of Earth Sciences,
Parks Road,
Oxford OX1 3PR, UK

Abstract

Sea level has risen on order of 100m since the Last Glacial Maximum (LGM), increasing the load on continental shelves and inducing lithospheric flexure. An analytic solution for the deflection of a linear slope due to sea level fluctuations is derived, based on a one-dimensional elastic plate model. This analytic solution provides deflection estimates of global continental shelves, due only to increases in water loading, effective elastic thickness (which is a proxy for the strength of the lithosphere with 2°×2°resolution) and the local shape of LGM continental margins (one-arc minute resolution). Changes in eustatic sea level are thus disengaged from changes in relative sea level. Variations in water loading can alter the slopes of continental shelves on the order of 30%, but importantly the magnitude is regionally variable. Hydro-isostasy adds to the magnitude of a sea level rise, long after the eustatic component of the sea level rise has ended. A sea-level rise will produce a steepening of a continental shelf. while a sea-level drop causes a decrease in shelf gradient and an increase in the total shoreline regression. Quantifying this effect is essential to reconstructing stream gradients, estimating sediment delivered by rivers, for estimating accommodation space through a sea level cycle, and to support the use of paleo-shoreline to estimate eustatic sea-level fluctuations.

Keywords:
Subsidence, Flexure, Continental Shelf, LGM

1. Introduction

The outermost layers of the Earth deflects in response to a load applied to it. One loading source might be the weight of a growing ice sheet. Another source, and the topic of this paper, is the increase in the weight of water overlying

flooded areas during a marine transgression. Sea-level rise over a continental shelf produces a wedge-shaped loading pattern that increases from the landward shoreline until it reaches its maximum at the lowstand shoreline. This asymmetric loading pattern causes a steepening of the shelf. A fall in sea level has a similar effect, but opposite in sign. The wedge-shaped unloading pattern, due to a sea-level drop, causes a decrease in shelf gradient and an increase in total shoreline regression. Quantifying this effect is essential to reconstruct, for instance, hypsometric drainage curves, stream gradients used to calculate paleo sediment delivery, or accommodation estimates during periods of different sea-level elevations. The amount of subsidence is also crucial for interpreting sea-level measurements. As a simple example, while the water depth of a paleoshoreline gives an estimate of relative sea-level change at that location, without an estimate of the amount of deflection at this location, eustatic sea-level change remains unknown.

The two main models used to predict deflections of Earth's lithosphere due to overlying loads are hydrostatic and flexural models ([3]; [24]). Hydrostatic models essentially treat the crust as a series of pistons placed alongside one another that operate independently. Such models assume that a load applied to a particular location is locally compensated for only by the mass directly beneath it ([2]; [17]). The governing equations for this type of model are easily solved to produce analytic solutions that can describe complex loading scenarios. Despite this however, their basic assumptions limit their use to large regions (for example, wavelengths greater than 400 km; [22]).

The second approach, the flexural model, assumes the lithosphere's response is more regional than local and can be modeled using an elastic plate that overlies a weak fluid substratum (e.g. Jeffreys, [8], [23]; [3]; [13]).

Typically, the upper crust is the plate that extends infinitely in all directions, while the lower crust and upper mantle form the elastic foundation. However, the elastic thickness acts as a proxy for the integrated strength of the entire lithosphere and so there could be be multiple brittle and ductile layers. In such models, a rigid lithosphere allows a load to be compensated by mass that is not directly below it. Typically, such models are more complex than their hydrostatic counterparts, but provide better predictions. Two-dimensional flexural models have had a wide range of success, ranging from identifying lithospheric bending beneath volcanic ocean islands and seamounts (e.g. [25]; [26]), large river deltas (e.g. [6]) and post-glacial rebound due to melting glaciers (e.g. [23]; [1]).

Our first goal is to present an analytic solution that solves the 1D flexure equation for a loading pattern that approximates that of sea-level rise (and fall) over a linearly dipping continental shelf. Although recent models solve more complex problems, such as viscoelastic deformations on a fully 3D Earth ([11]; [14]; [26]), our goal is different. A simple analytic solution, using a limited number of easily attainable input parameters, quantifies the first order affects of water-load induced subsidence on coastal regions.

Our second goal is to apply the analytical solutions to real-world examples. In particular, we predict what affect sea-level rise may have had on the seafloor

of the Adriatic Sea. In addition to providing an estimate of the seafloor at the LGM, the analytic approximation is compared to a numerical model that solves the full equation using real bathymetric data. As a second test, we apply the analytic model to all of Earth's continental shelves. Using a global bathymetric dataset ([10]), we calculate present-day shelf slopes, and widths. This allows us to calculate shelf slope at the LGM (given some simplifying assumptions), and the amount of eustatic sea-level change that produced today's shelves. We further show how changes in shelf gradient impact sediment delivery by rivers that cross the shelf during lowered sea level.

2. The Governing Equation

For this paper, we use an elastic plate model to predict deflections of Earth's lithosphere under loading. For a load distribution that varies in only one direction, the elastic flexure equation becomes

$$D\frac{d^4w}{dx^2} + N\frac{d^2w}{dx^2} + \Delta\rho g w = q(x) \tag{1}$$

where w is deflection from a datum, x is distance (perpendicular to loading), D is flexural rigidity, N is interplate force, q is load distribution, g is acceleration due to gravity, and $\Delta\rho$ is density difference between the material that underlies the flexed plate and the material that infills the flexure of the surface of the plate. The two right-most terms in Equation (1) represent local isostatic balance. The flexural rigidity (first) term reflects the stiffness of the lithosphere, which causes a load to be felt non-locally. The second term adds a component to the total deflection due to inter-plate stress. For our analysis will assume this contribution is negligible ([3]).

We do not derive the solution of the elastic flexure equation, as it is beyond the scope of this paper. The interested reader can find detailed derivations in [9], [13], or [22]. Our derivation makes four basic assumptions: (1) the lithosphere has a linear elastic rheology, (2) the deflections are small, (3) the elastic lithosphere is thin compared to the horizontal dimensions of the plate, and (4) planar sections within the plate are planar after deflection. Because the lithosphere is linear (assumption (1)), the resulting deflection due to multiple (or distributed) loads is calculated by integrating over these loads.

The non-dimensional parameters are,

$$\overline{x} = \frac{x}{\alpha},\ \ \overline{w} = \frac{\Delta\rho g}{q_0}w,\ \ \overline{q} = \frac{q}{q_0} \tag{2}$$

where the flexural parameter, α, is defined as,

$$\alpha \equiv \sqrt[4]{\frac{4D}{\Delta\rho g}} \tag{3}$$

and q_0 is the maximum load due to some sea-level rise or fall. With these substitutions, Equation (1) is,

$$\frac{d^4\overline{w}}{d\overline{x}^4} + 4\overline{w} = 4\overline{q} \tag{4}$$

For a line load of magnitude q_0 applied at the origin of an infinite plate ($q(\overline{x} = q_0\delta(\overline{x})$), the solution of Equation (4) is,

$$\overline{w}(\overline{x}) = \varepsilon e^{-|\overline{x}|} \left(\cos|\overline{x}| + \sin|\overline{x}|\right) \tag{5}$$

where ε is the half-width of the impulse function. Although in practice true line loads are not encountered, this solution of the flexure equation is important in constructing deflections due to arbitrary distributed loads. To do this, we take advantage of the fact that the flexure equation is linear with x. Thus, the sum of any number of specific solutions is also a solution.

3. The deflection of a continental shelf due to sea-level rise and fall

To apply the solution presented by Equation (4), to a continental slope that experiences loading (or unloading) due to sealevel rise (or fall), a loading pattern is constructed to approximate this change in load overlying the shelf. The first assumption is that the continental shelf is a linearly dipping plane and that we are measuring deflections along a dip profile. The assumption that continental shelves are linear is examined later, along with how the solution applies to non-linear shelves. For now though, we construct a loading pattern for a rise in eustatic sea level over a linear shelf.

The increase in the water-load resulting from a rise in sea level felt by an infinite slope is (Figure 1A),

$$\overline{q}(\overline{x}) = \begin{cases} 0 & \overline{x} < 0, \\ \overline{x} & 0 \leq \overline{x} < 0, \\ \overline{x}_0 & \overline{x} \geq \overline{x}_0 \end{cases} = R_{\overline{x}_0}(\overline{x}) \tag{6}$$

Thus, the water load is zero at the origin and increases linearly (with unit slope) until $\overline{x} = \overline{x}_0$, after which the load is constant. Integrating the line load solution (Equation (5)) over this distributed load gives an equation of the deflection of a linear shelf due to a rise in sea level (Figure 1C),

$$\overline{w}(\overline{x}) = \frac{1}{4\overline{x}_0}\left(F(\overline{x}) - F(\overline{x} - \overline{x}_0) + 4R_{\overline{x}_0}(\overline{x})\right) \tag{7}$$

where we define the function $F(x)$ as,

$$F(x) = e^{-|x|}\left(\cos|x| - \sin|x|\right) \tag{8}$$

3.1. Water loading

This non-dimensional equation (Equation (7)) gives the shape of the deflection due to rising (and falling) sea level. For a rise in eustatic sea level of Δz_e, one can dimensionalize the deflection through Equation (2) with $q = \rho_w g \Delta z_e$. Here we use Δ_w to non-dimensionalize deflection because water is filling deflections. Since the initial shelf is linear (with gradient S_0), the change in eustatic sea level relates linearly to the amount of transgression as $\overline{x}_0 = \frac{\Delta z_e}{S_0}$.

When the initial slope is deflected due to this increase in water loading, accommodation is increased. During transgression, water fills the new space created by subsidence and so further increases the load on the shelf. To model this important feedback, the specific gravity contrast ($\Delta\rho$) in Equation (1) is set as,

$$\Delta\rho = \rho_m - \rho_w \tag{9}$$

where ρ_m and ρ_w are density of the mantle and water, respectively. This is only an approximation, since it assumes that only water fills deflections. In reality, deflections on land will be filled with air (and perhaps, ultimately, sediment), and so the limit of this approximation will be most evident landward of the new (highstand) shoreline.

3.2. Water unloading

The unloading of the shelf due to falling sea level is similar (but opposite in sign) to the loading pattern of rising sea level (Equation (6); Figure 1B). Unlike the sea-level rise case, either water or air will fill deflections. We account for this be redefining the maximum load (q_0), the regression distance (x_0), and the density contrast ($\Delta\rho$). The maximum load in Equation (6) is located at the new (low-stand) shoreline, x_0. This is the position of the land-water interface after sea-level fall and uplift have been accounted for. The load at this position is,

$$q_0 = -\rho_w g \Delta z_r \tag{10}$$

where Δz_r is the relative change in sea level at the low-stand shoreline ($x = x_0$). This loading pattern accounts for water-filled deflections. Further deflections due to this unloading are assumed to be filled with air, and so the specific gravity difference is,

$$\Delta\rho = \rho_m \tag{11}$$

This assumes that the specific gravity of air is much less than that of Earth's mantle.

3.3. New shoreline position

In the absence of sedimentation, sea-level rise necessarily results in shoreline transgression. Likewise, falling sea-level forces a regression. In both instances, deflections due to the change in water loading will act to augment either the transgression or regression. From Equation (7) uplift is of primary importance to the amount of regression, although the amount of transgression is not greatly affected by subsidence.

For sea-level rise over a linearly dipping profile, the amount of transgression is the sum of that due to eustatic sea-level rise ($\overline{x}_0$) and water-load induced subsidence ($\delta\overline{x}$). Applying deflections from Equation (7) to a linear profile gives a solution for the portion of transgression due to water loading,

$$\begin{aligned} \delta\overline{x} &= \frac{\sigma_\uparrow}{4}\left(F(\delta\overline{x}) - F(\delta\overline{x} + \overline{x}_0)\right) \approx \frac{\sigma_\uparrow}{2(2+\sigma_\uparrow)}\left(1 - F(\overline{x}_0) + O^2(\delta\overline{x})\right) \\ \sigma_\uparrow &= \frac{\rho_w}{\rho_m - \rho_w} \end{aligned} \tag{12}$$

Under the same circumstances, a sea-level drop results in a regression that is the sum of that due to eustatic sea-level change and uplift caused by water unloading. Deflections from Equation (7) added to a linear profile provide a solution for the amount of regression due to the uplift that results from sea-level fall. We express this increase as $\delta\overline{x}$,

$$\begin{aligned} \Delta\overline{x} &= \sigma_\downarrow \overline{x}_0 + \frac{\sigma_\downarrow}{4}\left(1 - F(\overline{x}_0)\right) \\ \sigma_\downarrow &= \frac{\rho_w}{\rho_m} \end{aligned} \tag{13}$$

Figure 2 plots the increase in transgression (Figure 2A) and regression (Figure 2B) normalized to the change in shoreline position due only to an adjustment in eustatic sea level. In each case, the dimensional form ($\alpha \approx 65$ km) of Equations (12) and (13) are plotted, for three initial shelf gradients over a range of eustatic sea-level changes. Figure 2A shows that increase in transgression (relative to eustatic transgression) is most evident for both small changes in sea level and on shallower shelves. In all cases, the transgression increase is less than (and typically, much less than) 25%. In fact, Equation (12) suggests that water-load induced subsidence added only a few percent to the transgression of much of Earth's shorelines since the last glacial maximum.

Figure 2B shows uplift due to water unloading has a significant impact on regression distances. For all cases, the removal of water load causes at least a 31% increase in the seaward movement of the shoreline. From Equation (13) we calculate the limiting value for large sea-level drops to be $\sigma_\downarrow$ (for this case we used $\sigma_\downarrow \approx 0.31$).

3.4. Average Slope of the New Profile

The asymmetrical loading resulting from a rise in sea level causes the shelf gradient to increase within the range of transgression. The slope of the profile at

more seaward positions is not significantly changed, as the local loading pattern approximates that of a uniform load. To determine the average shelf gradient that results from such a loading pattern, we apply deflections of Equation (7) at $\overline{x} = 0$ and $\overline{x} = \overline{x}_0$ to a shelf that dips linearly with gradient $\overline{S}_0$. Doing this gives an expression for the average gradient following subsidence ($\overline{S}_1$),

$$\frac{\overline{S}_1}{\overline{S}_0} = 1 + \sigma_\uparrow + \frac{\sigma_\uparrow}{2\overline{x}_e}\left(F(\overline{x}_e) - 1\right) \tag{14}$$

In a similar manner, Equation (7) provides a solution for the reduction of slope due to uplift caused by water unloading. The slope of the shelf will be reduced by an amount,

$$\frac{\overline{S}_1}{\overline{S}_0} = 1 - \frac{\sigma_\downarrow}{2\overline{x}_0}\left(F(\overline{x}_0) - 1 + 2\overline{x}_0\right) \tag{15}$$

Figure 2 (C and D) plots the dimensional versions of the above two equations for slope amplification (shelf gradient following sea-level change normalized to initial gradient). As expected, rising sea level causes the shelf to become steeper, while falling sea-level results in shallower shelves. In both cases, the result of adjusting sea level is more pronounced on shelves with shallower initial gradients. From Equation (14) shelf steepening asymptotes to $1 + \sigma_\uparrow$ (or approximately 1.45) for large sea-level changes. Large sea-level drops cause shelf gradients to shallow to approximately 69% (1-$\sigma_\downarrow$) of their initial value.

3.5. Increase in Accommodation

Accommodation is critical to the amount of erosion and sediment delivery to an adjacent continental margin. Terrestrial accommodation is created or destroyed when the top of the fluvial/coastal plain system subsides below or is uplifted above the "theoretical equilibrium profile", defined as a graded or dynamic surface upon which there is no net sediment accumulation or erosion ([16]; [18]). The effect of base (sea) level change on fluvial systems depends upon factors such as rate of change, amount of change, direction of change, river character, and dynamics and erodibility of the sediment source area ([19]).

Without subsidence or sedimentation, an increase in base level results in greater total accommodation. The total amount of water increases and so is able to accommodate a larger amount of sediment. For a linearly dipping plane (with gradient $\overline{S}_0$), the total accommodation up to a distance $\overline{x}$ from the shoreline is,

$$A = \int_0^{\overline{x}} \overline{S}_0 \overline{x} \mathrm{d}\overline{x} = \frac{1}{2}\overline{S}_0 \overline{x}^2 \tag{16}$$

Thus, by increasing the upper limit of the integration, a rise in sea level increases the total amount of accommodation. This is deceiving though since much of this new accommodation is far from the shoreline where sediment cannot reach. In fact, for a linear slope, there is no change in accommodation near to the shoreline. However, water-loading induced subsidence will cause an increase in proximal accommodation.

Integrating Equation (16) over the transgression distance gives the contribution of water-load induced flexure to shelf accommodation,

$$\Delta A = \int_0^{\overline{x}} \overline{w}(\overline{x})\mathrm{d}\overline{x} = \frac{1}{2\overline{x}_0}\left(e^{-\overline{x}_0}\sin(\overline{x}_0) - \overline{x}_0^2 - 1\right) \rightarrow \frac{\Delta A}{A} \approx \sigma_{\uparrow}\left(1 - \overline{x}_0^2\right) \quad (17)$$

As we have shown, when sea-level falls the uplift due to water unloading causes the slope over this distance to decrease. However, the slope landward of the new shoreline is not significantly changed. Thus, water unloading has caused little change in the amount of accommodation seaward of the shore. However, the amount of landward accommodation changes significantly. Over the region of sea-level fall, the change in accommodation is,

$$\Delta A = \int_0^{\overline{x}} \overline{w}(\overline{x})\mathrm{d}\overline{x} = \frac{1}{2\overline{x}_0}\left(e^{-\overline{x}_0}\sin(\overline{x}_0) - \overline{x}_0^2 - 1\right) \rightarrow \frac{\Delta A}{A} \approx \sigma_{\downarrow}\left(1 - \overline{x}_0^2\right) \quad (18)$$

Thus, to first order, the accommodation is reduced by a factor of $\sigma_{\downarrow}$.

4. Time-dependence

Lithospheric deflections due to sea-level changes are a function of time as well as load ([13]). The two main causes are time-varying sea-level curves, and the response time of the lithosphere.

As sea level rises or falls from one shoreline to another, the water-loading pattern of the shelf also changes with the transgression (or regression). Ignoring subsidence for a moment, a change in sea level (η) on a linear shelf (with gradient) will cause the shoreline to move a distance, ξ,

$$\xi(t) = \frac{\eta(t)}{\overline{S}_0} \quad (19)$$

Using the coordinate system for rising sea level, ξ is equivalent to $\overline{x}_0$. However, the origin now moves in response to the changing sea level. Thus, Equation (7) is rewritten in a coordinate system whose origin is fixed to the starting shoreline position,

$$\overline{w}(\overline{x},t) = \frac{1}{4\overline{\xi}}\begin{cases} F\left(\overline{x}-\overline{\xi}\right) - F(\overline{x}) + 4R_{\overline{\xi}}\left(\overline{x}+\overline{\xi}\right) & \text{rising sea level,} \\ F\left(\overline{x}\right) - F\left(\overline{x}-\overline{\xi}\right) + 4R_{\overline{\xi}}(\overline{x}) & \text{falling sea level} \end{cases} \quad (20)$$

Figure 7A shows the response of three points to a linearly rising sea level. To dimensionalize Equation (20), a uniform rise in sea level of 120 m over a shelf with gradient 0.001 is considered. Figure 7A plots deflections at the positions of the initial (solid) and final (dash-dot) shorelines, as well as the halfway point (dashed). Although the initial shoreline position responds quickly to rising sea level, the signal takes significantly longer to be seen at the other two locations.

In fact, a landward-propagating forebulge initially causes a small amount of uplift at more inland positions. The time dependence of these curves is purely a result of a time-varying sea-level change.

Time-varying subsidence curves also result from the response time of Earth's lithosphere. After a load is applied, the lithosphere slowly relaxes as the viscous asthenosphere moves to make way for the deflection. The thermal and mechanical properties of the lithosphere are not taken into account and the lithosphere is assumed to ride passively on the viscous substrate. Although this relaxation time is a function of the asthenosphere's viscosity, we parameterize it through a relaxation time, λ. Using this parameterization, the deflection becomes ([15]),

$$w(\bar{t}) = \left(1 - e^{-\bar{t}}\right) w_\infty \tag{21}$$

where $\bar{t}$ is elapsed time since the load was applied (non-dimensionalized by the relaxation time), and w_∞ is the equilibrium deflection. Since the governing equation (Equation (1)) is linear, the deflection due to additional loads is a sum of their separate deflections. If loads are continuously applied over $0 < \bar{t}_0 < T$, the deflection is,

$$w(\bar{t}) = \int_0^T w_\infty(\bar{t}_0) \left(1 - x^{-(\bar{t}-\bar{t}_0)}\right) H_{\bar{t}_0}(\bar{t}) \mathrm{d}\bar{t}_0 \tag{22}$$

where $H_{\bar{t}_0}$ is the Heaviside step function (with a unit step at $\bar{t}_0$). Although we cannot solve this equation for a general $w_/infty$, we consider the specific examples of linear and sinusoidal loading. If the total applied load increases linearly at rate m, Equation (22) yields deflection as a function of time,

$$w(\bar{t}) = m \begin{cases} e^{-\bar{t}} + \bar{t} - 1 & \bar{t} \leq T, \\ e^{-\bar{t}} + T - e^{-(\bar{t}-T)} & \bar{t} > T, \end{cases} \tag{23}$$

Figure 7B shows the deflections with time for two loading situations that apply the same amount of weight. The load represented by the solid line in Figure 7B is applied over twice the amount of time as the dashed line. For the slower loading rate, the lithosphere comes closer to reaching its equilibrium deflection when the loading ends (in this case, 80% compared to 63%). The amount of deflection at the end of a loading period is expressed as,

$$w(T) = w_\infty \left(1 + \frac{e^{-T} - 1}{T}\right) \tag{24}$$

As an example, consider a lithosphere with a relaxation time of 2500 years. If we assume that sea level rose at a constant rate over a time of 12,000 years, Equation (22) estimates the deflection at the end of this period to be approximately 79% of its equilibrium amount.

For a sinusoidal forcing function with frequency, a, the deflection as a function of time becomes,

$$w(\bar{t}) = \frac{w_\infty}{a^2+1} \begin{cases} ae^{-\bar{t}} - a\cos(a\bar{t}) + \sin(a\bar{t}) & \bar{t} \le T \\ ae^{\bar{t}} \left(1 - e^T \left(\cos(aT) + a\sin(aT)\right)\right) \left(a^2+1\right) \sin(aT) & \bar{t} > T \end{cases} \tag{25}$$

Figure 7C shows lithospheric deflection (solid line) for sinusoidal forcing with a wavelength of about 7800 years (dashed line). The response of the lithosphere lags the forcing by about 1400 years. This lag is a function of the frequency of the forcing sine curve,

$$\Delta\bar{t} = \frac{1}{a}\left(\tan^{-1}\left(-\frac{1}{a}\right) + \frac{\pi}{2}\right) \tag{26}$$

Figure 7D shows this lag time (normalized to a relaxation time of 2500 years) for a range of wavelengths (solid line). For long-wavelength forcing, the lag time approaches 1 (the relaxation time). However, an increase in frequency causes a decrease in lag time that approaches zero. Using the lag time from Equation (26), the maximum amplitude of the response curve (Equation (25)) is expressed as a function of frequency,

$$w_{\max}(a) = \frac{1}{a^2+1}\left(\sin(a\bar{t}) - a\cos(a\bar{t})\right) \tag{27}$$

Figure 7D plots the attenuation (dashed line) of the forcing signal for a range of wavelength (assuming a relaxation time of 2500 years). The attenuation is the maximum deflection normalized to the equilibrium deflection. Low-frequency forcing allows the lithosphere to respond by closely approaching its equilibrium value. For long-wavelength forcing, on the order of hundreds to thousands of years, the lithosphere hardly responds at all (less than 20%).

We have so far only considered the viscosity of the asthenosphere and so have not taken into account therefore the possibility of any load-induced relaxation that might take place in the lithosphere itself. For example, oceanic flexure studies suggest that there is a reduction in the thickness of the mechanical layer that supports a load as the lithosphere relaxes from its short-term (seismic) thickness to its long-term elastic thickness. Depending on the relaxation time, which may vary regionally, the lithosphere may contribute an additional time-dependent flexure to the water load/unload flexure.

5. Application

In the following sections, some general ways that the derived analytic solutions can be applied to real-world situations are discussed. Two case studies are provided where the model is applied to reconstruct paleo-bathymetry.

5.1. Reconstruction a sea-level curve

Given a modern profile with the locations and ages of paleo-shorelines, one is able to construct a sea-level curve that will pass through these points at the

correct times. The resulting curve is a measure of the rise and fall of relative sea level at the (moving) shoreline. As an example of how such a sea-level curve would change with the inclusion of water loading induced subsidence consider Figure 4.

The present-day profile (solid line) is given with the time and location of a paleo-shoreline (point A). The rise in relative sea level over this time is the current water depth. In the absence of subsidence, this rise is equivalent to the change in eustatic sea level. However, the rise in sea level caused the initial profile (dashed line) to subside. The change in relative sea level is expressed as,

$$\Delta\overline{z}_r(\overline{x}) = \Delta\overline{z}_e + \overline{w}(\overline{x}) \tag{28}$$

Relative sea level is a function of $\overline{x}$ due to the uneven water loading. If point A represents a paleo-shoreline, then one can solve for the eustatic sea-level rise that created this profile. Solving for Δz_e at $\overline{x} = \overline{x}_0$, provides the eustatic change in sea level that produced the observed relative sea-level change,

$$\Delta\overline{z}_e = \frac{1}{\sigma_\uparrow} - \frac{1}{4\overline{x}_0}\left(F\left(\overline{x}_0\right) + 4\overline{x}_0 - 1\right) \tag{29}$$

Figure 2 E and F plots relative sea level change (at the lowstand shoreline) as a function of a change in eustatic sea level. The dimensional form of Equation (29) is plotted for three initial shelf slopes. Despite the seemingly complex form of Equation (29), the ratio of relative to eustatic sea level is nearly constant (approximately $1 + \sigma_\uparrow$).

If A were not a shoreline, but rather some arbitrary water depth, the problem becomes more difficult. We generalize Equation (29) to,

$$\Delta\overline{z}_e = \frac{1}{\sigma_\uparrow} - \frac{1}{4\overline{x}_0}\left(F\left(\overline{x}_A\right) + F\left(\overline{x}_A - \overline{x}_0\right) + 4\overline{x}_0\right) \tag{30}$$

Point A is no longer a shoreline, so that $\overline{x}_0$ is now unknown and one cannot solve explicitly for Δz_e. However, as noted previously (Equation (7)), sea-level rises do not cause significant changes in slope seaward of the low-stand shoreline. Thus, one can estimate the position $\overline{x}_0$ using the present-day slope along with the paleo-water depth of point A.

The case of reconstructing a falling sea-level curve is slightly different. For instance, if point A is now the current (low-stand) shoreline, and point B is a paleo-shoreline from some higher sea level, then the difference in elevation of these two points is roughly the same as the drop in eustatic sea-level. This is because the highstand shoreline saw only small deflections (Equation (12)). Thus, when reconstructing a falling sea level curve, the high-stand shoreline provides a nearly stationary datum from which one can make eustatic sea-level measurements. The amount of deflection at the upper shoreline ($\overline{w}(0)$) relative to the measured change in sea level gives an estimate of the error (ε) for such a measurement,

$$\varepsilon = \frac{\overline{w}(0)}{\Delta\overline{z}_e - \overline{w}(0)} = \overline{w}(0) \tag{31}$$

Equation (7) provides an expression for $\overline{w}(0)$ as a function of the non-dimensional distance between high-stand and low-stand shorelines ($\overline{x}_0$).

5.2. The Adriatic Since the LGM

Water loading on the Adriatic Sea due to sea-level rise since the last glacial maximum provides an example of how the presented analytic solutions can be used in a real-world situation, how accurate it is despite a non-linear shelf, and how it compares to the full (numerical) solution.

The northern part of the Adriatic Sea has a gently dipping shelf with water depths of less than 100m. This extends for about 250km, until the bathymetry steepens into a small basin, the Mid Adriatic Deep. Figure 5A shows a representative profile of the Adriatic that begins at the Po River delta and continues south until the beginning of the Mid Adriatic Deep (red curve). Thin Quaternary deposits litter the shelf ([21]). From these strata, [20] estimate the LGM shoreline to have been at a water depth of approximately 120m.

The green curve of Figure 5A is a linear approximation of the Adriatic shelf. With this approximated shelf, Equation (7) provides the change in eustatic sea level that produced the observed the change in relative sea level of 120m. Figure 5B shows the approximated shelf (green line) with this relative sea level drop. For comparison, Figure 5B also shows the result of a numerical model that solves the flexure equation for irregular bathymetry (red line). Both models show close agreement in the overall slope of the shelf. However, the two solution methods disagree slightly in the amount of eustatic sea-level change needed to produce the observed relative sea-level change. The numerical model and Equation (7) predicted a eustatic sea-level change in 93m, and 80m, respectively. The 13m difference is attributable to the deviation of the actual bathymetry from a linear plane, especially near the lowstand shoreline.

The analytic approximation provides a quick and easy method to predict the general seafloor shape given a change in sea level. In the case of the Adriatic, [12] take this process a step further and use the numerical model Sedflux to account for both water weight and the weight of the thin Quaternary deposits. Although the details of the estimated paleo-bathymetry differ, the analytic approximation captures the general profile shape.

5.3. The Steepening of Global Shelves Due to Sea-Level Rise

Our analytic model is applied to all of Earth's continental shelves in a way similar to the Adriatic tests. However unlike those tests, the large size of the input data prohibits the use of the numerical solution for comparison. The General Bathymetric Chart of the Oceans (GEBCO; [10]) provides digitized bathymetry for the World's Oceans at a scale of one arc-minute (approximately 2 km). Applying our approximation to these data, we estimate the contribution of water loading to the steepening of continental shelves.

To use Equation (15) to estimate the change in shelf slope, we first measure the slopes and widths of all the present-day continental shelves. Starting at each coastal pixel, the downstream path is followed until a maximum in bathymetric

curvature is found. The collection of points along this path defines a continental shelf. The distance between the two end points defines the shelf width, and a linear regression through these elevations estimates the average shelf slope. This procedure provides us with over 250,000 continental shelves, each with their own width and slope.

Figure 6 shows histograms of measured shelf width (A), gradient (B), and the R^2 value for the linear regression (C). The density function of shelf width is approximately exponential with a maximum at about 60km (this is somewhat artificial since we ignored shelves that contained fewer than 25 points). For our analysis, the shelf width defines the amount of transgression since the last glacial maximum ($\overline{x}_0$ in Equation (15)).

The distribution of shelf gradient is approximately lognormal with a mean of -3.4 (approximately 0.3 m/km). The large, gently dipping arctic shelves contribute to the two spikes around -4 and -4.3. The projection of the GEBCO dataset ([10]) results in a stretching of the coastlines closer to the poles, and so this procedure identifies a larger number of coastal pixels per unit length of coastline.

In Figure 6C we estimate the linearity of the continental shelves of the world. This is important in testing our initial assumption that sea-level rise occurs over a linearly dipping profile. Over 60% of the identified shelves show R^2 values greater than 0.7. For this study, we consider only those profiles that fall into this category.

Cross-shore distance, $\overline{x}_0$, in Equation (15) is non-dimensionalized with respect to the flexure parameter, α (Equation (3)). Thus, the change in shelf slope will also depend on the regional value of the flexural parameter. Crustal thickness, H, is related to flexural rigidity, D, and so α becomes a function of crustal thickness,

$$D = \frac{H^3 E}{12\left(1-\nu^2\right)} \Rightarrow \alpha^4 = \frac{H^3 E}{3\Delta\rho g\left(1-\nu^2\right)} \tag{32}$$

where ν is Poisson's ratio (0.25), and E is Young's modulus (7×10^{10} Nm^{-2}). The crust-2.0 model ([5]) predicts global crustal thickness on a $2^\circ \times 2^\circ$grid for the globe (Figure 7). This, along with Equation (15), estimates the flexural parameter for Earth's continental shelves.

With these data, we solve for the shelf slopes (S_{LGM}) at the LGM given the measured shelf widths ($\overline{x}_{\mathrm{LGM}}$),

$$\frac{S_{\mathrm{LGM}}}{S_{\mathrm{HS}}} = 1 - \frac{\sigma_\downarrow}{2\overline{x}_{\mathrm{LGM}}}\left(F\left(\overline{x}_{\mathrm{LGM}}\right) - 1 + 2\overline{x}_{\mathrm{LGM}}\right) \tag{33}$$

We non-dimensionalize the transgression distance with $\alpha = 60$ km, and use $\sigma_\downarrow = 0.31$. Figure 8 shows the ratio of LGM slope to current shelf slope. The purple areas show the extent of glaciers at LGM as predicted by ICE4G. Because ice loading induced subsidence was significant in these regions, with analysis has limited applicability. The steeper shelves along tectonically active margins show the least change, while the large shelves of passive margins show a reduction of

up to 70% of present-day values. This is, however, only an estimate of the effect of water-load induced subsidence, as no effort has been made to include effects of either thermal subsidence or subsidence from ice or sediment loading.

We know from flexure studies that α and, hence, the elastic thickness, varies regionally (Figure 7). We have assumed in our calculations $\alpha = 60$ km, which corresponds to an elastic thickness of ≈ 23 km. Figure 7 shows that elastic thickness varies spatially with some continental margins having low elastic thickness and others high. It is therefore useful to examine the effects of spatial variations in elastic thickness on the recovery of LGM shelf width and slope. Figure 9 shows how one can translate present-day shelf width (normalized to the flexure parameter, α) to LGM shelf gradient. For wide shelves (relative to α) we see that their LGM-gradients were only 70% of what they are today. Such cases are typical of passive margins such as those along the east coast of North America. Because narrow shelves undergo nearly uniform deflections across their width, their slopes do not change significantly with water loading. Active margins such as those off of Japan are examples of regions that fall into this category.

5.4. Sediment Delivery to Continental Margins During Lowered sea Level

Rivers transport a bed-material load, which involves sedimentary particles that are intermittently in contact with the channel bed. There are many theoretical-empirical steady-state formulae used to calculate this transport rate. For example a modified [4] bedload transport is a linear function of river gradient. The Einstein-Brown equation ([7]) gives the volumetric (total) sediment discharge as a function of the square (≈ 2.1) of the river gradient. Thus the up to 30% less steep shelf gradients that rivers crossed during the LGM period must be taken into account when modeling the sediment delivery to a LGM coastal zone. The analytical solution provided above could be readily incorporated into Landscape Evolution Models (e.g. [7]) employed for LGM simulation of Pleistocene landscape dynamics.

6. Summary

An analytic solution to the 1D flexure equation to approximate lithospheric deflections on a continental shelf that result from changes in sea level is presented. Although the model is not complex, it isolates and quantifies the first order response of continental shelves to water loading. From the analytic solution, approximations that predict the change in specific shelf properties due to sea level changes is derived. In particular, the change in shelf gradient is quantified, along with the intensification of either a transgression or regression. Although the contribution of subsidence to shoreline transgression is minimal, its impact on transgression is significant. Because of the model's simplicity, these relations provide researchers the ability to obtain quick first-order reconstructions of paleo-surfaces without having to run a complicated numerical model.

Because of the speed of the analytic solution, we apply the model to all of Earth's continental shelves. Using a global bathymetric dataset, the slopes and widths of present-day continental shelves are determined along with an estimate of the effect of sea level rise since the last glacial maximum on shelf slope worldwide. Results indicate that water loading since the Last Glacial Maximum may have had little impact on narrow shelves along active margins. However, along wider shelves typical of passive margins, increases in shelf gradient may reach 30%.

7. Notation

D	Flexural rigidity, 10^{23} Nm
w	Deflection, m
x	Position, m
x_0	Position of lowstand shoreline, m
δx	Additional transgression due to subsidence, m
Δx	Additional regression due to subsidence, m
$\Delta\rho$	Difference in density of mantle and fill material, kg m^{-3}
ρ_m	Density of mantle, 3.36×10^3 kg m^{-3}
ρ_w	Density of sea water, 1.05×10^3 kg m^{-3}
g	Acceleration due to gravity, 9.81 m s^{-2}
q	Load, N m^{-3}
S_0	Initial shelf gradient, –
S_1	Final shelf gradient, –
W	Present-day shelf width, m
Δz_e	Change in eustatic sea level, m
Δz_r	Change in relative sea level, m

Any symbol with an overbar is the non-dimensional version of the corresponding symbol in the above list. In all cases, quantities are non-dimensionalized through Equation (2).

Figures

Figure 1: Distributed load used to represent loading (unloading) of a shelf due to sea-level rise (A) and fall (B). (C) Deflection due to sea-level rise over a linear shelf (Equation (7)). Deflection due to sea-level fall is identical but opposite in sign (uplift, rather than subsidence).

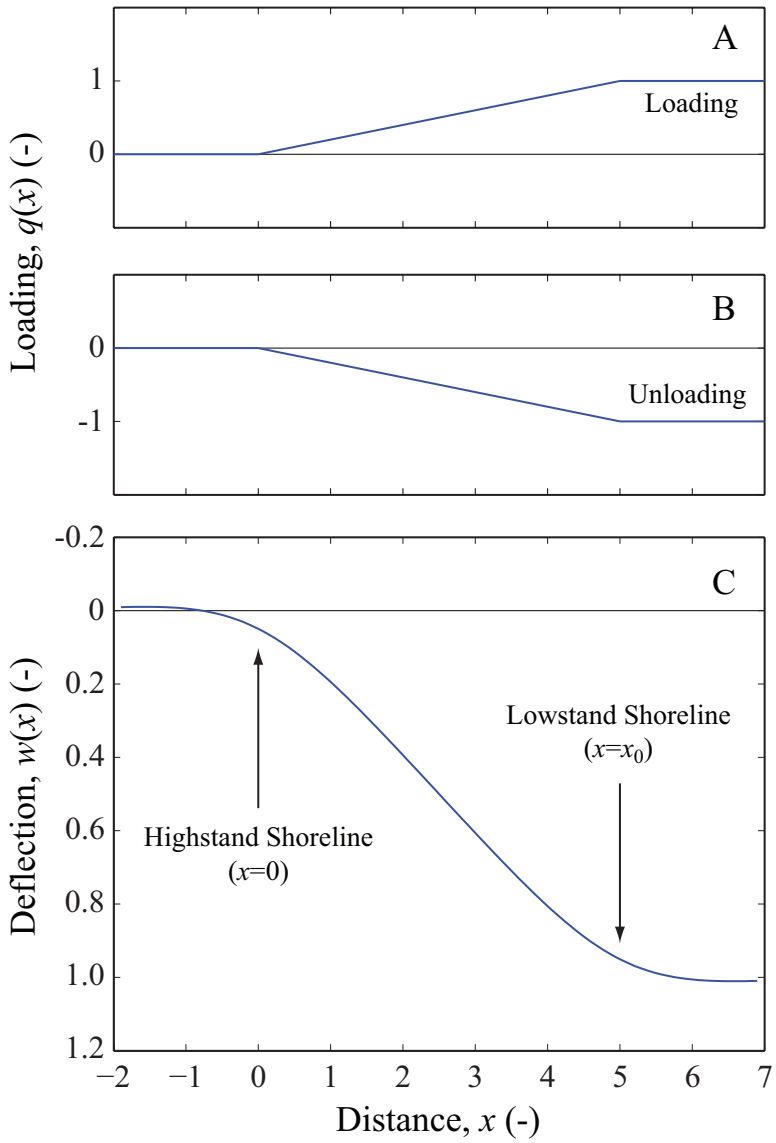

Figure 2: Analytic solutions for flexure of a linear shelf due water loading for sea-level rise and fall with $\alpha \approx 65$ km. Three initial shelf gradients are considered: 0.01 (dash-dot), 0.001 (dot), and 0.0001 (solid). For sea-level change over linear shelves, the contribution of water-load induced subsidence to shoreline transgression (A) and regression (B). Amount of increased shoreline change is normalized to total change in shore position. Although subsidence contributes little to regression, uplift resulting from water unloading accounts for between 30% and 50% of total regression. Panels C and D plot fractional change in shelf gradient resulting from sea level rise (C) and fall (D). Final shelf slope is normalized to its value before sea-level adjustment. Panels E and F show change in relative sea level is nearly linear with change in eustatic sea level. Here we measure relative and eustatic change in sea level at a low-stand shoreline that results from sea-level rise (E) and fall (F).

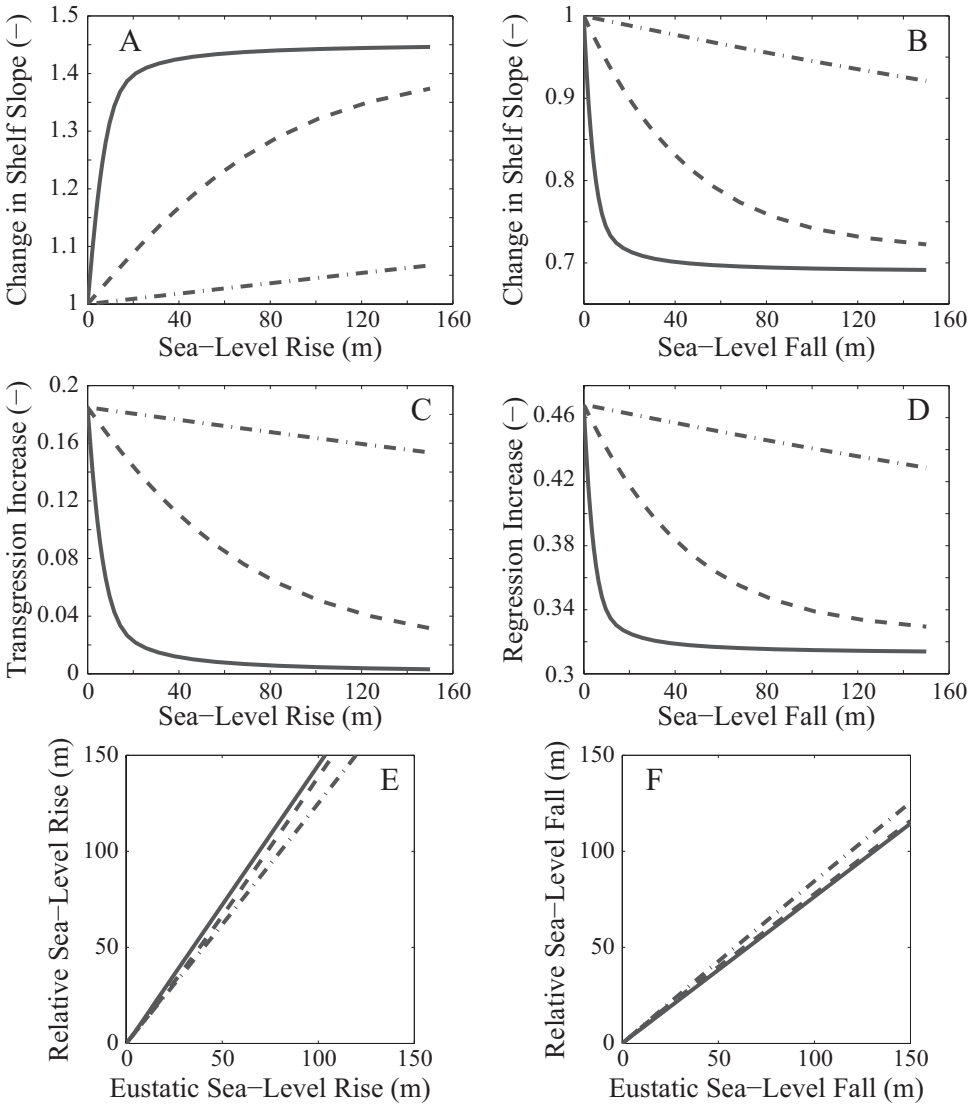

Figure 3: Deflection is a function of time due to time varying sea-level curves and lithospheric relaxation time. (A) Time-varying deflection of three points along a shelf as sea level rises at a constant rate. Lowstand shoreline (solid line) subsides nearly linearly from onset of sea-level rise. Point located at the middle of the transgression (dotted line) and eventual highstand shoreline (dot-dashed line) responds more slowly as transgression proceeds. (B) Loading of dashed line is applied twice as quickly as solid line. (C) Deflection (solid line) lags forcing (dotted line) and is attenuated. (D) Lag time (solid line) and attenuation (dotted line) as a function of wavelength of forcing sine function.

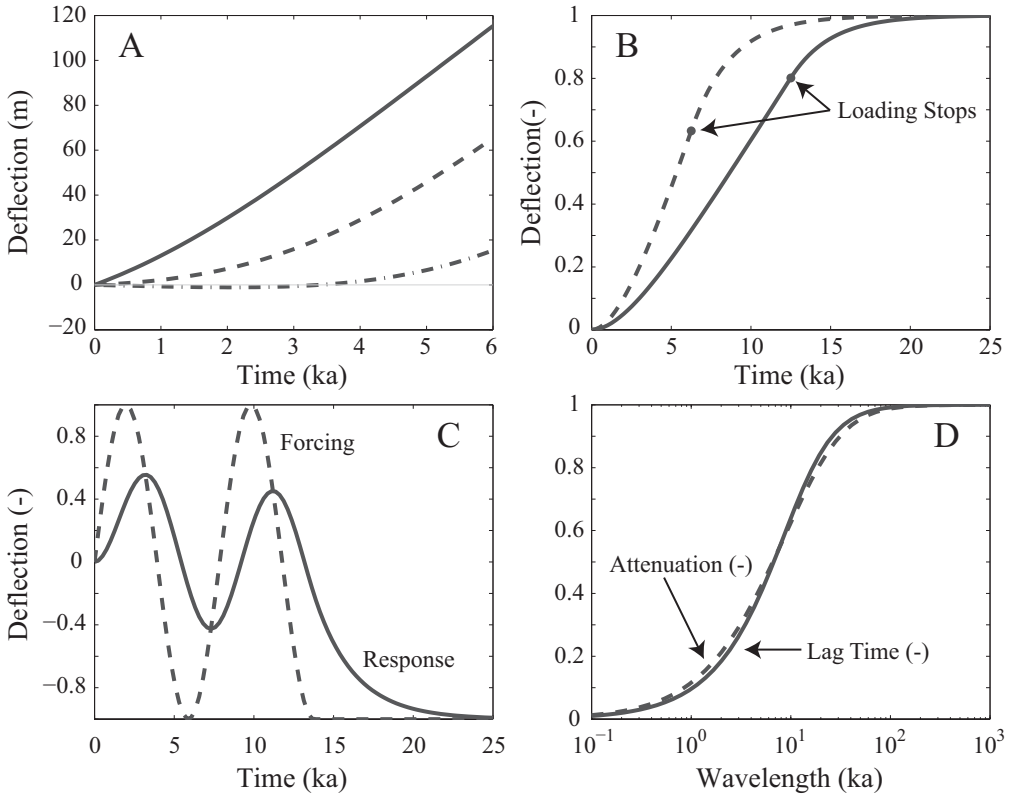

Figure 4: Sketch of how a shelf responds to rising sea level. Dashed line shows initial sea floor with shoreline at x=x0 (point A). Sea-level rise causes shoreline transgression from point A to point B, and resulting increase in water loading causes subsidence of Point A.

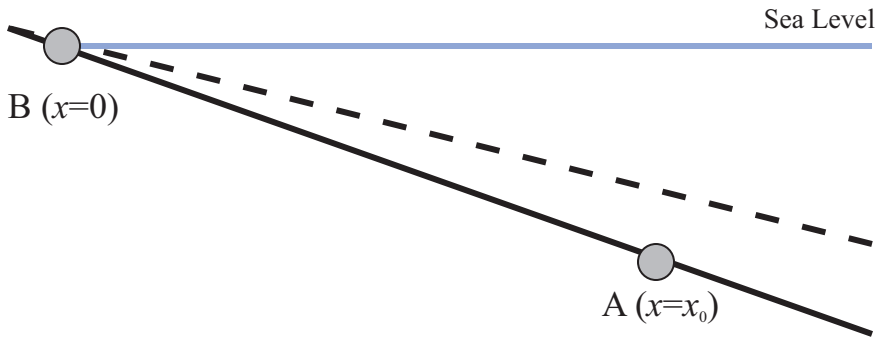

Figure 5: Numerical experiments that attempt to reconstruct seafloor of the Adriatic at LGM. Panel (A) presents current bathymetry (red line) of the Adriatic and a linear approximation (green line). Panel (B) compares LGM bathymetry of analytic solution (green line) to numerical solution (red line) assuming a relative drop in sea level of 120m.

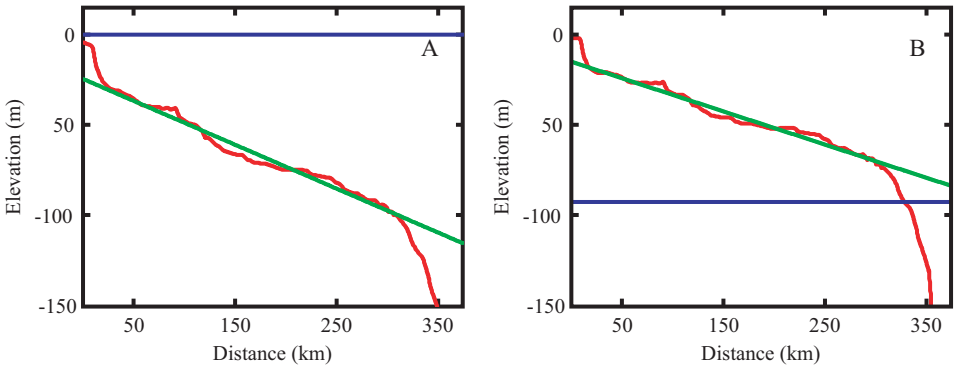

Figure 6: Histograms of measured shelf properties obtained from GEBCO global bathymetric data. Shelf widths (A) form an exponential density function. Shelf gradients (B) are approximately log-normal with mean of -3.3. Over half of measured shelves display an R^2 value of greater than .8 to a linear regression (C).

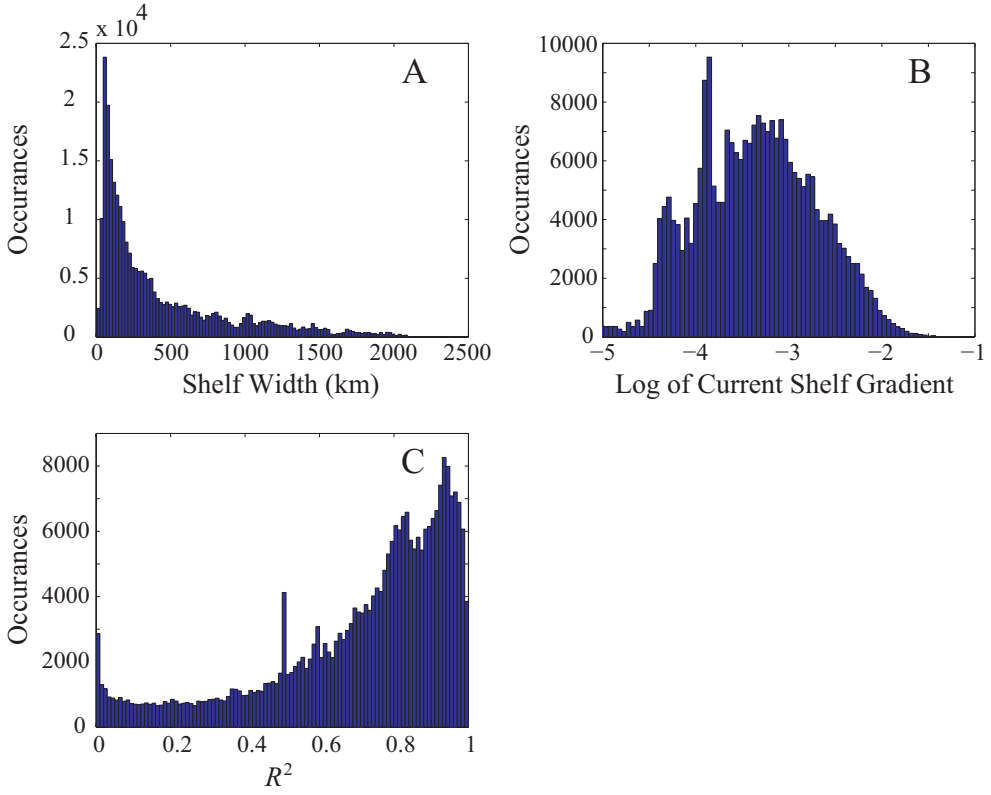

Figure 7: Global map of effective elastic thickness on a 2°by 2°grid. Distribution of effective elastic thickness along continental margins are narrowly centered at 30 km.

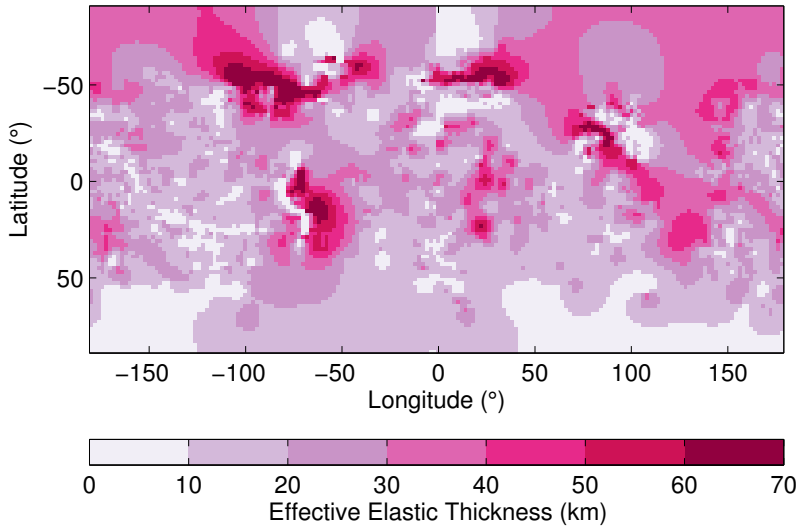

Figure 8: Estimate of shelf-slope change due to increased water loading of Earth's shelves since LGM. Purple areas indicate ice cover at LGM. Gradients of wider shelves were up to 70% less than that of today. Slopes of narrower shelves, especially those along active margins, were not significantly impacted.

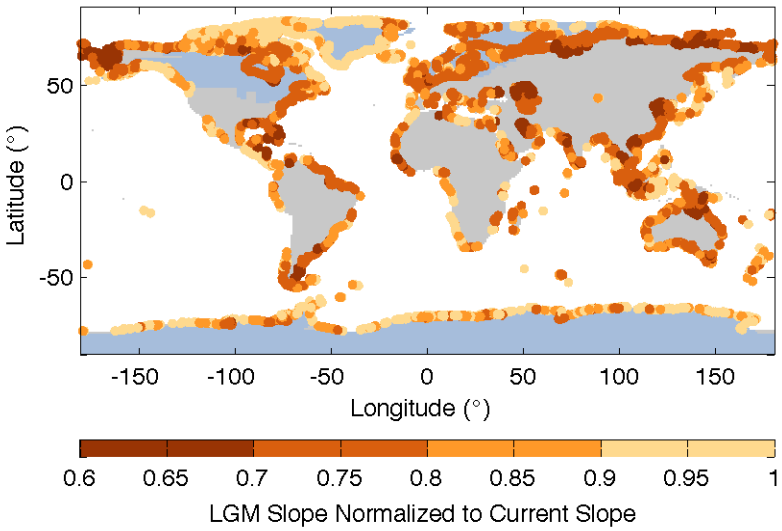

Figure 9: The change in the gradient of present-day shelves since the last glacial maximum is a function of their width normalized to the flexure parameter, α. At LGM, the gradient of wide shelves ($\overline{W} > 10$; New Jersey shelf, for example) were 70% of their current values, while narrow shelves see no change ($\overline{W} < .1$; Japan, for example)

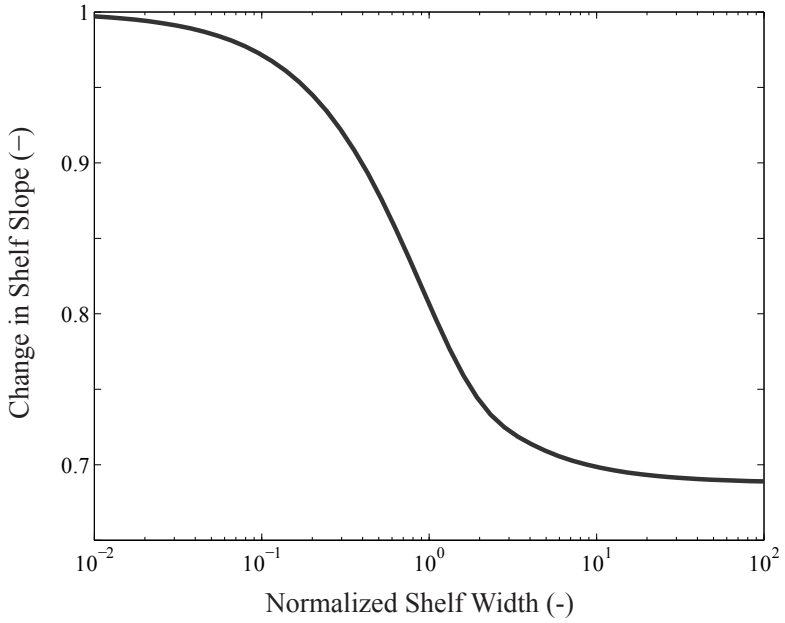

References

[1] A Paulson, S. Z., Wahr, J., 2005. Modelling post-glacial rebound with lateral viscosity variations. Geophys. J. Int. (163), 357–371.

[2] Airy, G. B., 1855. On the computation of the effect of the attraction of mountain-masses as disturbing the apparent astronomical latitude of stations in geodetic surveys. Philosophical Transactions of the Royal Society of London 145, 101–104.

[3] Angevine, C. L., Heller, P., Paola, C., 1990. Quantitative sedimentary basin modeling: American association of petroleum geologists. Tech. Rep. 32, The American Assosiation of Petroleum Geologists, Tulsa, OK, shortcourse Note Series.

[4] Bagnold, R. A., 1966. An approach to the sediment transport problem from general physics. U.S. Geological Survey Professional Paper 422-I, 37.

[5] Bassin, C., Laske, G., Masters, G., 2000. The current limits of resolution for surface wave tomography in north america. In: EOS Transactions. Vol. 81.

[6] Cochran, J. R., 1973. Gravity and magnetic investigations in the guiana basin, western equatorial atlantic. Geol. Soc. Am. Bull. 84, 3249–3268.

[7] Fagherazzi, S., Howard, A. D., Wiberg, P., 2004. Modeling fluvial erosion and deposition on continental shelves during sea level cycles. J. Geophys. Res. 109.

[8] Gunn, R., 1944. A quantitative study of the lithosphere and gravity anomalies along the atlantic coast. Franklin Inst. J. 237, 139–154.

[9] Hetényi, M., 1979. Beams on Elastic Foundations, 11th edition. The University of Michigan Press, Ann Arbour.

[10] IOC, IHO, BODC, 2003. Centenary edition of the gebco digital atlas. published on CD-ROM on behalf of the Intergovernmental Oceanographic Commission and the International Hydrographic Organization as part of the General Bathymetric Chart of the Oceans, Liverpool, U.K.

[11] Kaufmann, G., Wu, P., Li, G., 2000. Glacial isostatic adjustment in fennoscandia for a laterally heterogeneous earth. Geophys. J. Int. 143 (1), 262–273.

[12] Kubo, Y., Syvitski, J. P. M., Hutton, E. W. H., Kettner, A. J., 2006. Inverse modeling of post last glacial maximum transgressive sedimentation using 2d-sedflux: Application to the northern adriatic sea. Marine Geology 234 (1-4), 233–243.

[13] Lambeck, K., 1988. Geophysical Geodesy: The Slow Deformations of the Earth. Oxford Univ. Press, Oxford, UK.

[14] Martinec, Z., Cadek, O., Fleitout, L., 2001. Can the 1d viscosity profiles inferred from postglacial rebound data be affected by lateral viscosity variations in the tectosphere? Geophys. Res. Lett. 23, 4403–4406.

[15] Peltier, W. R., 1998. Postglacial variations in the level of the sea: implications for climate dynamics and solid-earth geophysics. Rev. Geophys. 36, 60389.

[16] Posamentier, H. W., Vail, P. R., 1988. Eustatic controls on clastic deposition II. No. 42. pp. 125–154.

[17] Pratt, J. H., 1855. On the attraction of the himalaya mountains and of the elevated regions beyond them upon the plumb-line in india. Philosophical Transactions of the Royal Society of London 145, 53.

[18] Schumm, S. A., 1991. River response to baselevel change: Implications for sequence stratigraphy. Journal of Geology 101, 279–294.

[19] Syvitski, J. P. M., Scott D Peckham, P. W., Howard, A., Driscoll, N., 2001. Predicting the distribution and properties of buried submarine topography on continental shelves. In: Hines, P. C., Makris, N. C., Holland, C. W. (Eds.), Geoclutter and Boundary Characterization 2001: Acoustic Interaction with the Seabed. pp. 67–71, technical Memorandum DREA TM-2001-185.

[20] Trincardi, F., Cattaneo, A., Asioli, A., Correggiari, A., Langone, L., 1996. Stratigraphy of the late-quaternary deposits in the central adriatic basin and the record of short-term climate events. In: Guilizzoni, P., Oldfield, F. (Eds.), Palaeoenvironmental analysis of Italian Crater lake and Adriatic sediments (PALICLAS). Vol. 55. pp. 39–70.

[21] Trincardi, F., Correggiar, A., Roveri, M., 1994. Late quaternary transgressive erosion and deposition in a modern epicontinental shelf: the adriatic semi-encolsed basin. Geo-Mar. Lett. 14, 41–51.

[22] Turcotte, D. L., Shubert, G., 1982. Geodynamics: Application of Continuum Physics to Geological Problems. Wiley, New York, NY.

[23] Walcott, R. I., 1970. Isostatic response to loading of the crust in canada. Can. J. Earth Sci. 7, 716–727.

[24] Watts, A. B., 2001. Isostasy and Flexure of the Lithosphere. Cambridge University Press, Cambridge, UK.

[25] Watts, A. B., Cochran, J. R., 1974. Gravity anomalies and flexure of the lithosphere along the hawaiian-emperor seamount chain. Geophys. J. R. Astr. Soc 38, 119–141.

[26] Zhong, S., Paulson, A., Waher, J., 2003. Three-dimensional finite-element modeling of earths viscoelastic deformation: effects of lateral variations in lithospheric thickness. Geophys. J. Int. 155 (2), 679–695.